SUPPORTING INFORMATION

3D-Addressable Redox: Modifying Porous Carbon Electrodes with Ferrocenated 2-nm Gold Nanoparticles

Kwok-Fan Chow,[#] Rajesh Sardar,[#,§] Megan B. Sassin,[†] Jean Marie Wallace,[✧] Stephen W. Feldberg,[$] Debra R. Rolison,[†] Jeffrey W. Long,[†] and Royce W. Murray[#,]*

[#] Kenan Laboratories of Chemistry, University of North Carolina, Chapel Hill, NC 27599

[$] Chemistry Department, Brookhaven National Laboratory, Upton, New York 11973

[†] Code 6170 Surface Chemistry Branch, U. S. Naval Research Laboratory, Washington, DC 20375

[✧] Nova Research, Inc., Alexandria, VA 22308

§ Present address: Dept. Chem. Chem. Biol., Indiana Univ./Purdue Univ., Indianapolis, IN 46202

[*] rwm@unc.edu

Experimental Details

Chemicals. Thioacetic acid (>98%), *t*-octylammonium bromide (Oct_4NBr, >98%), sodium borohydride ($NaBH_4$, >98%), *t*-butylammonium hexafluorophosphate (Bu_4NPF_6, puress), from Aldrich and toluene (reagent grade), acetonitrile (Optima), methylene chloride (HPLC grade), tetrahydrofuran (HPLC grade), and ethanol (HPLC grade) from Fisher were used as received. The gold precursor, $HAuCl_4\ xH_2O$ (from 99.999% pure gold), was synthesized using a literature procedure and stored in a freezer at –20°C. Water was purified using a Barnstead NANOpure system (18 MΩ). Ferrocene hexanethiol (HSC6Fc) was synthesized by refluxing a mixture of (1.11 g, 3.17 mmol) ω-bromohexane ferrocene and thiourea (0.600 g, 7.88 mmol) in ethanol (50 mL) overnight. The reaction mixture was neutralized with NaOH (aq), refluxed for a further 3 h, acidified with HCl to pH ~2, diluted with water, and extracted with CH_2Cl_2, thoroughly washing the organic extract phase with water. The material obtained after rotary evaporation of the CH_2Cl_2 product solution was chromatographed on silica gel with ethyl acetate/hexanes. The ^{1}H NMR (400 MHz, CD_2Cl_2) of the thiol gave the appropriate NMR peaks: δ) 4.0 (m, 9 H), 2.49 (q, J) 7.2 Hz, 2 H), 2.30 (t, J) 7.6 Hz, 2 H), 1.56 (m, 2 H), 1.46 (m, 2 H), and 1.32 (m, 5 H) ppm with no dithiol peaks present and no significant line broadening, indicating that the

ferrocene groups were in the reduced state.

MPC Synthesis. $Au_{225}(SC6Fc)_{43}$ was synthesized as previously reported.[S-1] Briefly, 3.19 g of $HAuCl_4$ $x H_2O$ dissolved in 100 mL of deionized water was mixed with 5.20 g of Oct_4NBr dissolved in 200 mL of CH_2Cl_2 and stirred for 30 min at room temperature, giving a clear aqueous phase and an orange-brown toluene phase. The separated organic phase was mixed and stirred for 20 min with added ω-ferrocenyl hexanethiol (2:1 ligand-to-Au mole ratio). The now colorless Au(I)-thiolate polymer solution was cooled to 0 °C and 3.8 g of $NaBH_4$ dissolved in 10 mL of water, also cooled to 0 °C, was added with vigorous stirring; the solution immediately turned black and some gas evolution occurs. The rapid stirring was continued for 1 h at 0 °C, after which the dark organic phase was collected and the solvent removed on a rotary evaporator at room temperature. The black solid suspension was stirred in 400 mL of acetonitrile for 6 h, and the solid product collected and washed with acetonitrile on a fine glass frit.

Microscopy and spectroscopy. High-resolution microscopy (HRTEM) images were collected using a JEOL 2010F-FAS instrument at 200 kV accelerating voltage. Scanning electron microscopy (SEM) micrographs were accrued using Hitachi S-4700 FESEM at 20 kV. The energy dispersive X-ray spectroscopic (EDX) was performed on Oxford INCA PentaFet-X3.

Solutions for ICP-MS analysis were obtained by digestion of a sample of $Au_{225}(SC6Fc)_{43}$–modified nanofoam in a mixture of 3.6 M HCl/1.4 M HNO_3, followed by dilution into 2% HNO_3. A Varian 820-ICPMS, Inductively Coupled Plasma Mass Spectrometer, was used for all elemental analysis measurements. The source has a MicroMist nebulizer, max flow rate of 0.4 mL min^{-1}, for sample introduction into the plasma. Standard plasma conditions (Power 1.4 kW, plasma flow 18.00 L min^{-1}, auxiliary flow 1.80 L min^{-1}, sheath gas flow 0.18 L min^{-1}, sampling depth 7.5 mm) were used. All solutions were prepared using 18 MΩ cm deionized water (lab supply) and trace metal grade Nitric Acid (Thermo Fisher Scientific Inc.). Instrument conditions were optimized using the auto-optimization feature of this instrument. Samples were introduced while setting the peristaltic pump at 3 rpm. The spray chamber was cooled to 3°C. Standards were prepared using ICP standards (Inorganic Ventures, Christiansburg, VA). In all measurements, a 5-ppb solution of indium was used as internal standard and mixed online with each sample through a tee.

Indium ion In^{115} (internal standard) (ion abbreviations and isotopes monitored) were monitored in a peak-hopping mode, using 50000 μs as dwell time, and measuring five replicates of an average of 20 data points. The standard curve included at least 8 concentration levels in the quantification range. The standard data set was fitted to a linear curve. The coefficient of correlation was 0.99 or better.

Percent errors in calculated concentrations were 15% or lower.

Electrochemistry. Cyclic voltammetry was done at room temperature using Pt wire and Ag/AgCl/3 M KCl (aq) counter and reference electrodes, respectively, in a three-electrode setup. Measurements were performed using a CH Instruments (Austin, TX) Model 760C electrochemical analyzer and a Pine Instruments (Durham, NC) WaveNow potentiostat.

Carbon Nanofoam Electrodes. Initial experiments were done using carbon nanofoam papers (MarkeTech, Port Townsend, WA, grade #1) which were pyrolyzed under constant argon flow (100 mL^{-1} min) in a tube furnace. Pyrolysis was achieved by ramping the temperature at 1 °C min^{-1} to 1000 °C, holding at 1000 °C for 2 h, and then ramping down at 1 °C min^{-1} to 25 °C. These locally prepared nanofoams were 0.017 cm in thickness with a density of 0.4 g cm^{-3}. Contacts were made by Type A and Type B mounting (Figure S-1A,B). The Type A nanofoam electrode had a geometrical area of 0.266 cm^2 exposed to the solution (accounting for solution exposure on both sides), a mass of 1.7×10^{-3} g, and a volume of 4.5×10^{-3} cm^3. These same quantities for the Type B mounted electrode were 0.133 cm^2 (the one side exposed), 1.7×10^{-3} g, and 4.55×10^{-3} cm^3. Later experiments were conducted on purchased, already-pyrolyzed carbon nanofoams (MarkeTech, grade 2) which were mounted as in Type C (Figure S-1C).

Carbon-fiber paper supported carbon nanofoams were also prepared as previously described.[S-2] Briefly, a 50 wt% resorcinol–formaldehyde (RF) aqueous sol, with a resorcinol-to-catalyst ratio of 1500, was prepared and oligomerized in a hood at room temperature for 3 h. Stacked plasma-etched commercial Lydall carbon fiber paper was vacuum infiltrated with the oligomerized RF sol, sealed in a glass slide assembly with duct-tape and foiled wrapped. After curing overnight at room temperature, the wet sol-infiltrated-carbon-fiber-papers were processed in a pressure cooker (Nesco 3-in-1 pressure cooker, Target) on the slow cook setting (88–94 °C) for 9.5 h, followed by the warm cycle (80 °C) for a total processing time of 24 h in the commercial cooker. After slow cooking, the packets were unwrapped and RF nanofoam papers submerged in water and rinsed for a few hours. The papers were then rinsed with acetone for 1–2 h and air dried. The RF nanofoam papers were heated under argon at 0.05 °C min^{-1} to 30 °C for 1 h and then at 1 °C min^{-1} to 1000 °C for 2 h to produce the conductive two-ply carbon nanofoam papers.

P**reparing contacts to nanofoams.** For Type A contacts, a square of the pyrolyzed nanofoam paper was contacted to an Al wire with protective rubber sleeve using silver paste, followed by curing at 70 °C overnight. The silver paste contact was coated completely with an epoxy and again cured overnight at 70 °C. For Type B contacts, a preweighed (3.3×10^{-3} g) 0.7×0.7 cm piece of pyrolyzed nanofoam paper

was cemented (electrodag, EB-012, Ladd Research, a graphite-based conductive material) to a roughened nickel foil having a corner tag for contact (see Figure S1,B) followed by 70°C oven curing for 2 h. The exposed Ni foil was covered with epoxy (except for the corner tag) and was cured overnight at 70°C. For Type C contacts, a piece of nanofoam was cemented (electrodag, EB-012) between two pieces of nickel foils with a hole (diameter 6.7 mm) punched on it. Epoxy was used to cover the exposed Ni foil and was cured overnight at 70°C. The nanofoam is exposed to solution on both sides of the electrode and the typical projected area of the exposed nanofoam is around 20 mm^2.

Loading nanoparticles into the nanofoams.

Type A nanofoam electrodes were soaked in 0.05 mM nanoparticle CH_2Cl_2 solutions for 24 h, then washed copiously with CH_2Cl_2 and transferred to 1.0 M Bu_4NPF_6/CH_2Cl_2 electrolyte for electrochemical measurements. Types B and C nanofoam electrodes were loaded similarly except the 0.05 mM nanoparticle solutions were in 0.1 M Bu_4NPF_6/THF and the soaking time—in an evacuated glass desiccator to encourage pore-filling—was 2 h. The electrodes were thoroughly washed with 0.1 M Bu_4NPF_6/THF and then soaked in nanoparticle-free 0.1 M Bu_4NPF_6/CH_3CN for 1 h, to remove the more resistive THF solution. The Type B and C electrodes were transferred to 1.0 and 2.0 M Bu_4NPF_6/CH_3CN electrolyte, respectively, for electrochemical measurements.

Simulations and comparisons to experimental CV.

The theoretical curves were generated using a modification of the theoretical expression discussed earlier[S-3,S-4]

$$i = \frac{a\left(v + \frac{i'}{\Delta t}R_u\right)\left(\frac{\gamma n^2F^2\Gamma_{total}}{RT}\frac{\exp\left[\frac{\gamma mF}{RT}\left(E_{app} - iR_u - E^0\right)\right]}{\left(1+\exp\left[\frac{\gamma mF}{RT}\left(E_{app} - iR_u - E^0\right)\right]\right)^2} + C_{dl}\right) + a\left(b\left(E_{app} - E^0\right) + b_0\right)}{1 + \frac{aR_u}{\Delta t}\left(\frac{\gamma n^2F^2\Gamma_{total}}{RT}\frac{\exp\left[\frac{\gamma mF}{RT}\left(E_{app} - iR_u - E^0\right)\right]}{\left(1+\exp\left[\frac{\gamma mF}{RT}\left(E_{app} - iR_u - E^0\right)\right]\right)^2} + C_{dl}\right) + abR_u} \quad (1)$$

where i' is the current (A) at time t, i is the current at $t = t + \Delta t$, a is area (cm^2), γ is an interaction parameter which we elucidate further , below[S-4] and b and b_0, terms added for the present work, shape

the background current,[S-4] v is the scan rate (V s^{-1}), Γ_{total} is the surface coverage (mol cm^{-2}), ΔE_{app} is the voltage step (V), R_u is the uncompensated resistance (ohms) and F, R, and T have their usual significance. For the simulations in the present work $\Delta E_{app} = \pm 0.0001$ V and therefore, for a cyclic voltammetric scan, $\Delta t = |\Delta E_{app}|/|v|$ s. When the potential, $E_{app,start} - E^0|$, is sufficiently negative (for the present work) the initial value of i' is i'_{start} defined by:

$$i'_{start} = \frac{a\left(b\left(E_{app,start} - E^0\right) + b_0\right)}{1 + abR_u} \qquad 2$$

The subsequent values of i for any given value of E_{app} incremented by $\pm \Delta E_{app}$ is easily obtained by solving eqn.1 iteratively initially setting all i-values on the rhs of eqn. 1 equal to i'; three iterations are sufficient for convergence (see detailed discussion in Ref. S-4). Two basic simplifications in the derivation of eqn. 1 are: 1. the electron transfers are reversible, and 2. the uncompensated resistance resides in the solution and not within the zone of confinement. Although the introduction non-unity values of the parameter γ in eqn. 1 may appear to effect non-thermodynamic behavior it is important to remember that the surface concentrations Γ_{ox} and Γ_{red} (where $\Gamma_{ox} + \Gamma_{red}$) are *concentrations* and not activities. Thus, as discussed in detail in a previous publication[S-4] eqn. 1 is thermodynamically self-consistent if the corresponding activities of the surface confined species are defined as

$$a_{ox}^{sc} = \left(\frac{\Gamma_{ox}}{\Gamma_{total}}\right)^{1/\gamma} \text{ and } a_{red}^{sc} = \left(\frac{\Gamma_{red}}{\Gamma_{total}}\right)^{1/\gamma} \qquad 3$$

Thus, if the effective potential of the working electrode is E_{we} (= $E_{app} - iR_u$) then

$$\frac{a_{ox}^{sc}}{a_{red}^{sc}} = \exp\left[\frac{nF}{RT}\left(E_{we} - E^0\right)\right] = \exp\left[\frac{nF}{RT}\left(E_{app} - iR_u - E^0\right)\right] \qquad 4$$

Combining eqns 3 and 4 gives:

$$\frac{a_{ox}^{sc}}{a_{red}^{sc}} = \left(\frac{\Gamma_{ox}}{\Gamma_{red}}\right)^{1/\gamma} = \exp\left[\frac{nF}{RT}\left(E_{app} - iR_u - E^0\right)\right] \qquad 5$$

Then:

$$\frac{\Gamma_{ox}}{\Gamma_{red}} = \exp\left[\frac{\gamma mF}{RT}\left(E_{app} - iR_u - E^0\right)\right] \qquad 6$$

This leads[S-3,S-4] to eqn. 1, a convenient formalism which we adopt in the present work in lieu of more detailed information regarding the possible interactions of the surface confined species. When $R_u = 0$, setting $\gamma = 1$ produces the classic peak shape for reversible electron transfer of a surface confined species[S-5] with full-width-half-max = 0.090 V when T = 298.2 KI; $\gamma > 1$ effects sharper peaks; $\gamma < 1$ effects broader peaks.

The protocol for "fitting" the simulated to experimental CVs was first to estimate the values of the simulation parameters which produced a satisfactory "eyeball" fit for the slowest scan rate (0.002 V s^{-1}) and then, for two higher scan rates, readjusting, if needed, only the values of C_{dl}, b and b_0; these values may have a complicated and non-quantifiable dependence on the scan-rate and on the electrode history. The emphasis for the fitting was on matching the shapes, positions and magnitudes of the faradaic peaks. The comparisons of these simulated CVs with their corresponding experimental CVs are shown in Figures 2–4 in the manuscript. All parameter values are given in the Figure legends.

References

S-1. Wolfe, R. L.; Balasubramanian, R.; Tracy, J. B.; Murray, R. W. *Langmuir* **2007**, *23*, 2247–2254.

S-2. Lytle, J. C.; Wallace, J. M.; Sassin, M. B.; Barrow, A. J.; Long, J. W.; Dysart, J. L.; Renninger, C. H.; Saunders, M. P.; Rolison, D. R. *Energy Environ. Sci.* **2011**, 4, 1913–1925.

S-3. Feldberg, S. W. *J. Electroanal. Chem.* **2008**, *624*, 45–51.

S-4. Feldberg, S. W. *Anal. Chem.* **2011**, *83*, 5851–5856.

S-5.. Bard, A. J.; Faulkner, L. R. *Electrochemical Methods*, 2nd ed.; Wiley: New York, 2001; pp 591.

(Type A)

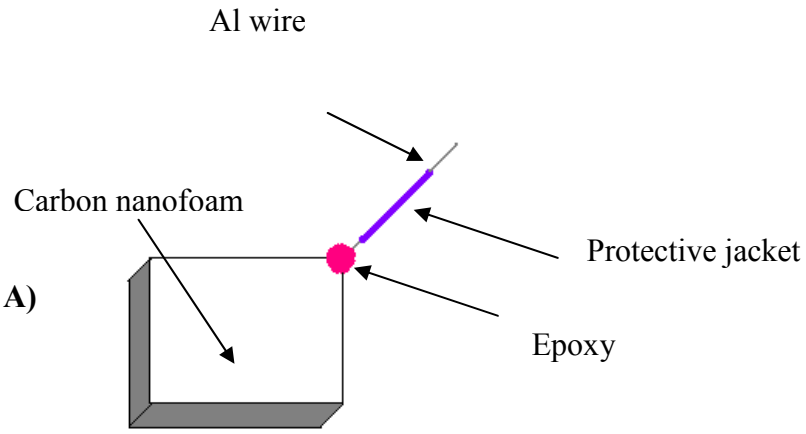

(Type B)

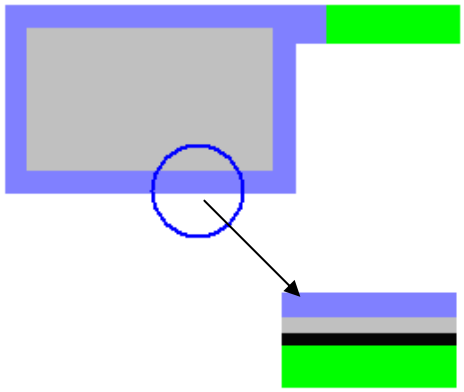

(Type C)

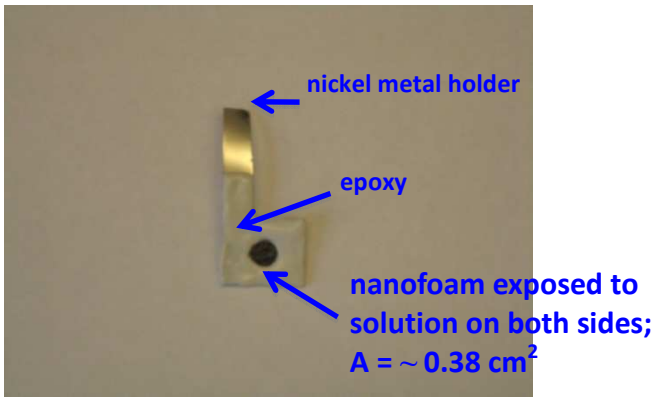

Figure S-1. Schematic diagrams of Types A, B, and C mounting of carbon nanofoam electrodes. Type A had a geometrical electrode surface area of 0.266 cm^2 (counting both exposed sides of the electrode); electrode thickness was 0.017 cm. Type B materials were Ni foil (green), electrodag conductive adhesive (black), carbon nanofoam (gray), and epoxy (blue). The exposed geometrical electrode surface area was 0.25 cm^2 and the carbon nanofoam was 0.017 cm thick. Type C had a geometrical area of 0.19 cm^2 (total 0.38 cm^2 counting both exposed sides) and a thickness of 0.017 cm.

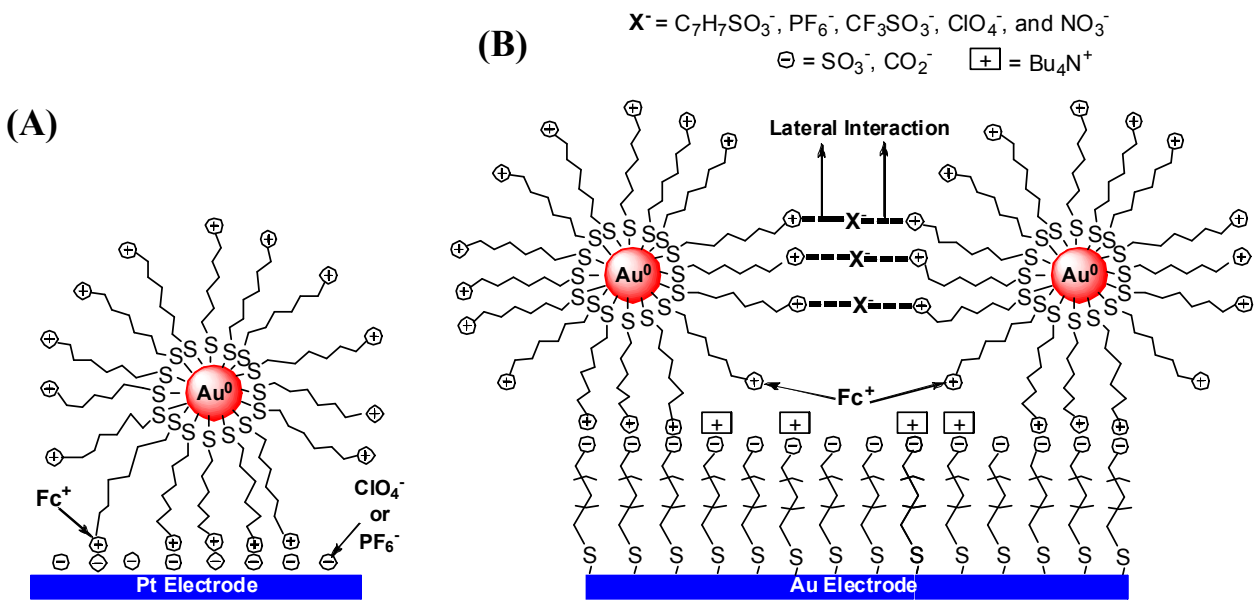

Panel A: Schematic representation of ion-induced adsorption of ferrocenium cation on bare Pt electrode surface. Ion-pair bridges are proposed to form between adsorbed electrolyte anions on the electrode surface and NPs. Panel B: Cartoon representing adsorption of NPs on a negatively charged SAM surface. The adsorption is promoted by lateral ion bridges between neighbor NPs.

Figure S-2. This figure is reproduced from *Anal. Chem.* **2009**, *81*, 6960–6965, for the convenience of the reader.